Technical Note

Effect of Nozzle Design on Bubbly Jet Entrainment and Oxygen Transfer Efficiency

Daniel D. Lima[1] and Iran E. Lima Neto[2]

Abstract: This study investigates experimentally the effect of nozzle type, including diffusers with single- and multiple-orifices with different diameters, on the hydrodynamics and mass transfer characteristics of air-water bubbly jets discharged at the bottom of a water tank. The results revealed that for the same flow rates of air and water, the total area of the orifices independent of the number of ports controls the initial momentum of the bubbly jets and the jet-to-plume length scale of the flow. An integral model was fitted to the experimental data in order to obtain entrainment coefficients for each test and at different water depths, which confirmed that merged multiple bubbly jets can be analyzed using an equivalent single jet integral model. This resulted in an entrainment relationship described as a function of the kinematic buoyancy flux, bubble slip velocity, and distance from the source, which is similar to that available in the literature for bubble plumes, but with different constants. Finally, the model proposed here is compared to previous models and applied to practical cases including mixing and aeration of tanks and water bodies, indicating that gas transfer efficiency can be significantly enhanced by using multiple-orifice arrangements. **DOI: 10.1061/(ASCE)HY.1943-7900.0001493.**

Author keywords: Aeration; Bubbles; Entrainment; Jets; Plumes.

Introduction

Jet aeration occurs when a gas-liquid mixture is injected with relatively high momentum in a liquid. These types of multiphase flows are encountered in many engineering applications such as artificial aeration and mixing in reactors, tanks, and water bodies (Sun and Faeth 1986; Iguchi et al. 1997; Zhang and Zhu 2014; Lima Neto 2012b, 2015). Contrastingly, bubble-plume aeration occurs when a gas is released in a liquid with negligible initial momentum (Milgram 1983; Seol et al. 2007; Lima Neto et al. 2008a, 2016). Compared to bubble-plume aeration, the injection of gas-liquid mixtures in water has advantages such as production of small bubbles without the need for porous diffusers (Lima Neto et al. 2008b, c), which is beneficial for gas-liquid mass transfer (Mueller et al. 2002). Moreover, gas injection into effluent diffusers can also be an attractive alternative for artificial aeration of water bodies (Lima Neto et al. 2007).

There is extensive literature on aeration systems for wastewater treatment and water quality amelioration in rivers, lakes, and reservoirs (Wüest et al. 1992; Mueller et al. 2002; Schierholz et al. 2006; Lima Neto et al. 2007; Pacheco and Lima Neto 2017). Nevertheless, most papers refer to bubble-plume aeration or horizontal/angled injection of gas-liquid mixtures in confined environments. The focus of this study is on the hydrodynamics and mass transfer characteristics of jet aeration systems composed of air-water bubbly jets injected vertically in stagnant water. Previous experimental studies on this subject have been performed by Sun and Faeth (1986), Kumar et al. (1989), Iguchi et al. (1997), and Lima Neto et al. (2008b), in which the two-phase flow structure induced by the bubbly jets was assessed for different flow conditions, tank geometries, and nozzle diameters. However, these studies were limited to single-orifice nozzles with relatively small diameters (up to 13.5 mm). Note that both multiple-orifice and larger nozzles are also common in jet aeration systems (Mueller et al. 2002). In the case of multiple orifices, the impact of merging jets on the flow structure of bubbly jets is also a problem that needs to be tackled. Past studies on single-phase jets, plumes, and bubble plumes have shown that after the jets have fully merged, the jet group could be considered as an equivalent single jet or plume (Freire et al. 2002; Kaye and Linden 2004; Lai and Lee 2012).

The hydrodynamics of vertical air-water bubbly jets in stagnant water has been investigated theoretically by using the integral approach of Lima Neto (2012b, 2015), which is based on the classical bubble plume theory and the entrainment hypothesis (Milgram 1983; Wüest et al. 1992; Lima Neto 2012a). Nevertheless, Lima Neto's model has been validated for bubbly jets discharged through single-orifice nozzles and with relatively high momentum at the source. Moreover, this model considers constant entrainment coefficients at different heights above the nozzle, and may not be representative of the flow structure under two-layer stratified water conditions, where the buoyancy flux changes at a density interface (Lima Neto et al. 2016), or under relatively deep-water conditions, where bubble size and slip velocity can vary significantly due to compressibility and mass dissolution effects (Lima Neto and Parente 2016).

This study investigates experimentally the influence of different diffusers, including single- and multiple-orifice and large nozzles on the two-phase flow structure of air-water bubbly jets in a still water tank. The integral model of Lima Neto (2012b, 2015) is also used as reference to estimate the entrainment coefficients for different flow conditions and at different heights above the diffuser, in order to obtain a comprehensive model that can be used for artificial aeration and mixing for different nozzle designs. Model simulations are also compared with previous integral models and the

[1]Ph.D. Student, Dept. of Hydraulic and Environmental Engineering, Federal Univ. of Ceará, Campus do Pici, bl. 713, 60.451-970 Fortaleza, Brazil.

[2]Assistant Professor, Dept. of Hydraulic and Environmental Engineering, Federal Univ. of Ceará, Campus do Pici, bl. 713, 60.451-970 Fortaleza, Brazil (corresponding author). Email: iran@deha.ufc.br

Note. This manuscript was submitted on July 14, 2017; approved on February 22, 2018; published online on May 30, 2018. Discussion period open until October 30, 2018; separate discussions must be submitted for individual papers. This technical note is part of the ***Journal of Hydraulic Engineering***, © ASCE, ISSN 0733-9429.

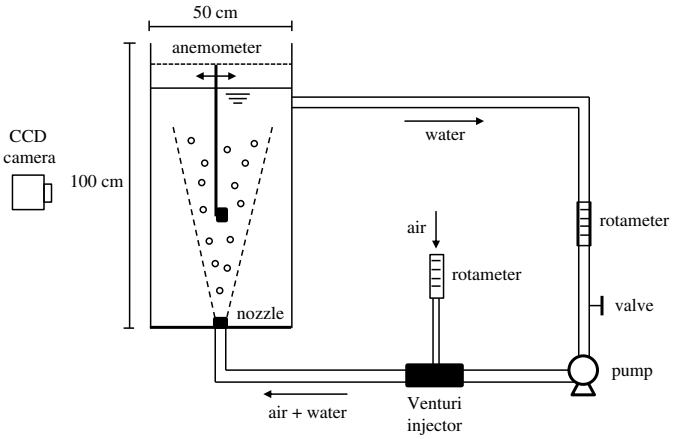

Fig. 1. Schematic of experimental setup.

impact of nozzle type on the oxygen transfer efficiency is also investigated.

Experimental Setup and Methods

The experiments were carried out in a square plexiglass tank, with a width of 50 cm on the sides and a height of 100 cm, as shown schematically in Fig. 1. The tank was filled with tap water up to a height of 80 cm. A centrifugal pump of 2.0 hp withdrew water from 5 cm below the water surface and then supplied a Venturi injector with a throat diameter of ¼ in. (see details in Lima Neto and Porto 2004) that incorporated air into a 1 in. -PVC pipeline. The resulting gas-liquid mixture was then injected at the base of the tank by using diffusers with different diameters (d) and numbers of orifices (n) (Fig. 2): nozzle A, with $n = 1$ and $d = 30$ mm; nozzle B, with $n = 1$ and $d = 10$ mm; nozzle C, with $n = 4$ and $d = 5$ mm; and nozzle D, with $n = 8$ and $d = 3.5$ mm. Note that the nozzles B–D had the same total area of the orifices. The volumetric flow rates of water (Q_l) and air (Q_g) were measured with rotameters. Different values of Q_l were adjusted through a globe valve. This resulted in different combinations of Q_l and Q_g for each nozzle design, as summarized in Table 1. Note that the gas flow rate was not independently controlled, as it was a result of the combination of nozzle design and liquid flow rate.

An electromagnetic propeller anemometer (MiniWater20, Omni Instruments, Dundee, UK) with relative error of 2% and detection range of 2–500 cm/s was used to measure the mean axial water velocity at distances z of 20, 35, and 50 cm from the nozzle exit, and at different radial positions r from the bubbly jet centerline. Images of the bubbles were also recorded by using a Nikon D70s charge-coupled device (CCD) camera (Nikon, Tokyo) with a resolution of 18 pixels/cm. Similar anemometers and cameras were used by Lima Neto et al. (2008a, b, c).

The software ImageJ (Schneider et al. 2012) was used to process the images of the bubbles. In order to minimize the error in estimating bubble size, images with significant overlapping of large bubbles were discarded. Twenty imagens with about 50–300 bubbles each were selected per experiment. The exposure area was used to calculate the equivalent-sphere diameter of each bubble. This allowed the computation of the bubble Sauter mean diameter per each experiment.

The gas-liquid flow ratio, bubble size, and radial distribution of axial water velocity at different heights were studied for each nozzle type and flow condition. Because of the detection limit of the anemometer (>2 cm/s), only velocity measurements above 20% of the centerline value were considered, which resulted in velocities larger than 5 cm/s for all the tests. The impact of multiple-orifice and nozzle diameter on the velocity profiles induced by bubbly jets was then investigated considering both dimensional and nondimensional frameworks. Gaussian distributions were also fitted to the velocity data by minimizing the sum of the squares of the deviations between measured and adjusted velocity profiles for each experimental condition. Following the same procedure, the integral model of Lima Neto (2012b) was also fitted to the measured velocity profiles in order to adjust the entrainment coefficient for each experiment.

The integral model of Lima Neto (2012b) is based on the following equations that account for conservation of mass (1) and momentum (2) along the bubbly jet:

$$\frac{d(\pi b^2 u_c)}{dz} = 2\pi b \alpha u_c \tag{1}$$

$$\frac{d(\pi b^2 u_c^2)}{dz} = \frac{2gQ_a H_a}{\gamma(H_a + H_d - z)(\frac{u_c}{1+\lambda^2} + u_s)} \tag{2}$$

in which u_c = centerline water velocity of the bubbly jet; b = bubbly jet radius where the axial water velocity $u = 0.37u_c$; z = vertical distance from the nozzle exit; α = entrainment coefficient; γ = momentum amplification factor due to turbulence; λ = spreading ratio of the bubble core with respect to the surrounding water flow; u_s = bubble slip velocity; Q_a = volumetric air flow rate at atmospheric pressure; H_a = atmospheric pressure head; and H_d = pressure head at the nozzle exit.

The numerical solution of Eqs. (1) and (2) using the Runge-Kutta fourth-order method gives centerline water velocities of the bubbly jets for different heights, and the radial velocity profile is obtained by

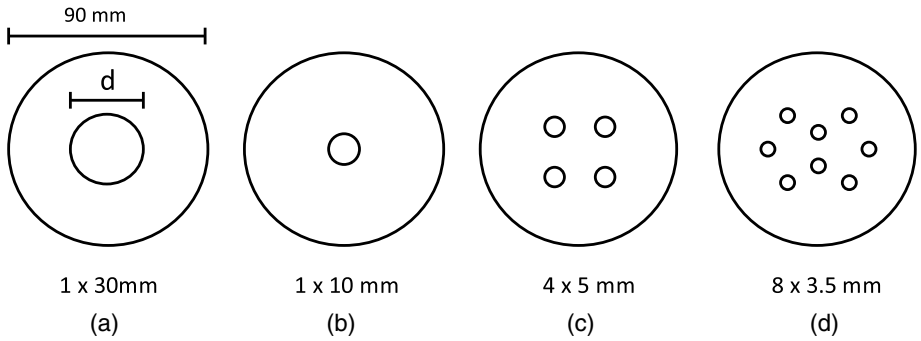

Fig. 2. Schematic of diffusers with different diameters (d) and numbers of orifices (n): (a) nozzle A, with $n = 1$ and $d = 30$ mm; (b) nozzle B, with $n = 1$ and $d = 10$ mm; (c) nozzle C, with $n = 4$ and $d = 5$ mm; and (d) nozzle D, with $n = 8$ and $d = 3.5$ mm.

Table 1. Experimental conditions for the tests with different nozzle diameters (d) and number of orifices (n)

Experiment	Nozzle	d (mm)	n	$Q_{l,o}$ (L/min)	$Q_{g,o}$ (L/min)	R_o	M_o (m^4/s^2)	B_o (m^4/s^3)	L_m (m)
1	A	30	1	12	1	9.20×10^3	6.13×10^{-5}	1.96×10^{-3}	1.56×10^{-2}
2	A	30	1	16	3	1.34×10^4	1.19×10^{-4}	2.62×10^{-3}	2.23×10^{-2}
3	A	30	1	18	4	1.56×10^4	1.56×10^{-4}	2.94×10^{-3}	2.57×10^{-2}
4	A	30	1	20	6	1.84×10^4	2.04×10^{-4}	3.27×10^{-3}	2.99×10^{-2}
5	A	30	1	22	9	2.19×10^4	2.68×10^{-4}	3.60×10^{-3}	3.49×10^{-2}
6	B	10	1	16	2	3.82×10^4	1.02×10^{-3}	2.62×10^{-3}	1.11×10^{-1}
7	B	10	1	20	4	5.09×10^4	1.70×10^{-3}	3.27×10^{-3}	1.46×10^{-1}
8	B	10	1	25	6	6.58×10^4	2.74×10^{-3}	4.09×10^{-3}	1.87×10^{-1}
9	C	5.0	4	11	1	1.27×10^4	4.67×10^{-4}	1.80×10^{-3}	7.49×10^{-2}
10	C	5.0	4	19	3	2.33×10^4	1.48×10^{-3}	3.11×10^{-3}	1.35×10^{-1}
11	C	5.0	4	25	4	3.08×10^4	2.56×10^{-3}	4.09×10^{-3}	1.78×10^{-1}
12	D	3.5	8	18	2	1.52×10^4	1.30×10^{-3}	2.94×10^{-3}	1.26×10^{-1}
13	D	3.5	8	22	3	1.89×10^4	1.98×10^{-3}	3.60×10^{-3}	1.57×10^{-1}
14	D	3.5	8	30	5	2.65×10^4	3.79×10^{-3}	4.91×10^{-3}	2.18×10^{-1}

applying a Gaussian distribution: $u = u_c[\exp(-r^2/b^2)]$, where r is the radial distance from the bubbly jet centerline. The initial conditions of water velocity (u_o) and radius (b_o) are given by Lima Neto (2012b)

$$u_o = \frac{Q_{l,o}}{(1-\varepsilon_0)(\pi\frac{d^2}{4})} \tag{3}$$

$$b_o = d \tag{4}$$

where $Q_{l,o}$ = volumetric flow rate of water at the nozzle exit; d = nozzle diameter; and ε_o = air volume fraction given as

$$\varepsilon_o = \frac{Q_{g,o}}{Q_{g,o} + Q_{l,o}} \tag{5}$$

where $Q_{g,o}$ = volumetric flow rate of air at the nozzle exit.

Note that for the cases of multiple-orifice nozzles, a reference diameter is needed to analyze the experimental results, normalize the data, and run the integral model. This will be discussed in the next section.

Assuming constant values of the spreading ratio of the bubble core ($\lambda = 0.6$), momentum amplification factor ($\gamma = 1.0$), and bubble slip velocity ($u_s = 0.23$ m/s), as usually done in bubble plume and bubbly jet studies (Lima Neto 2012a, b), the entrainment coefficient (α) was adjusted by least squares fitting of the model to the radial water velocity profiles measured at $z = 20$, 35, and 50 cm.

The entrainment coefficients fitted for each experiment and height above the nozzles were plotted as a function of dimensionless parameters in order to find a general correlation that could be used for both single- and multiple-orifice nozzles with different diameters.

Finally, model simulations were performed to predict the induced flow rates in tanks/water bodies and for comparison with previous integral models. Moreover, the following equation given by Lima Neto and Parente (2016) was used in combination with Eqs. (1) and (2) to assess the axial variation of mass of gaseous species transferred per bubble to the water:

$$\frac{dm_i}{dz} = -K_L(HP_i - C_i)\frac{\pi d_b^2}{(\frac{u_c}{1+\lambda^2} + u_s)} \tag{6}$$

in which m_i = mass of each gaseous specie i (i.e., oxygen or nitrogen); K_L = liquid-side mass-transfer coefficient; H = Henry's constant; P_i = partial pressure of the gas at a given depth; C_i = bulk aqueous-phase concentration; and d_b = bubble diameter. Relationships for K_L, H, P_i, and u_s were obtained from Wüest et al. (1992). This allowed a comparison of the effect of different nozzle types on the standard oxygen transfer efficiency (SOTE), which is defined as the mass fraction of oxygen supplied that is actually dissolved into the water (Mueller et al. 2002; Schierholz et al. 2006; Lima Neto et al. 2007).

Results and Discussion

Fig. 3 shows the gas-liquid flow ratio $Q_{g,o}/Q_{l,o}$ obtained for each experimental condition (Table 1). Overall, the values of $Q_{g,o}/Q_{l,o}$ obtained in this study ranged from about 0.1 to 0.4 and were similar to those reported by Baylar and Ozkan (2006) and Baylar et al. (2007). Comparing the results for Experiment 4 (nozzle A, with a 30-mm diameter) and Experiment 7 (nozzle B, with a 10-mm diameter), it is clearly seen that the smaller the orifice diameter, the lower the values of $Q_{g,o}/Q_{l,o}$. The same trend has been observed by comparing other pairs of experiments (e.g., 2 and 6, 3 and 12, 5 and 13). This occurred because smaller orifices produce larger minor head losses and, consequently, less air incorporation into the Venturi injector. On the other hand, the experiments with the multiple-orifice nozzles C (4 × 5 mm) and D (8 × 3.5 mm) resulted in similar values of $Q_{g,o}/Q_{l,o}$, but lower than those obtained with the single-orifice nozzle B. This implies that minor head losses at nozzles C and D were higher than those at nozzle B, even though these three nozzles had the same total area of the orifices.

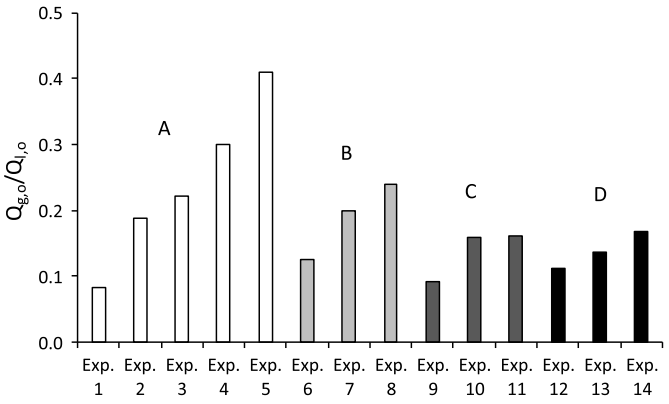

Fig. 3. Gas-liquid flow ratio obtained for each nozzle type (A, B, C, and D) and experimental condition.

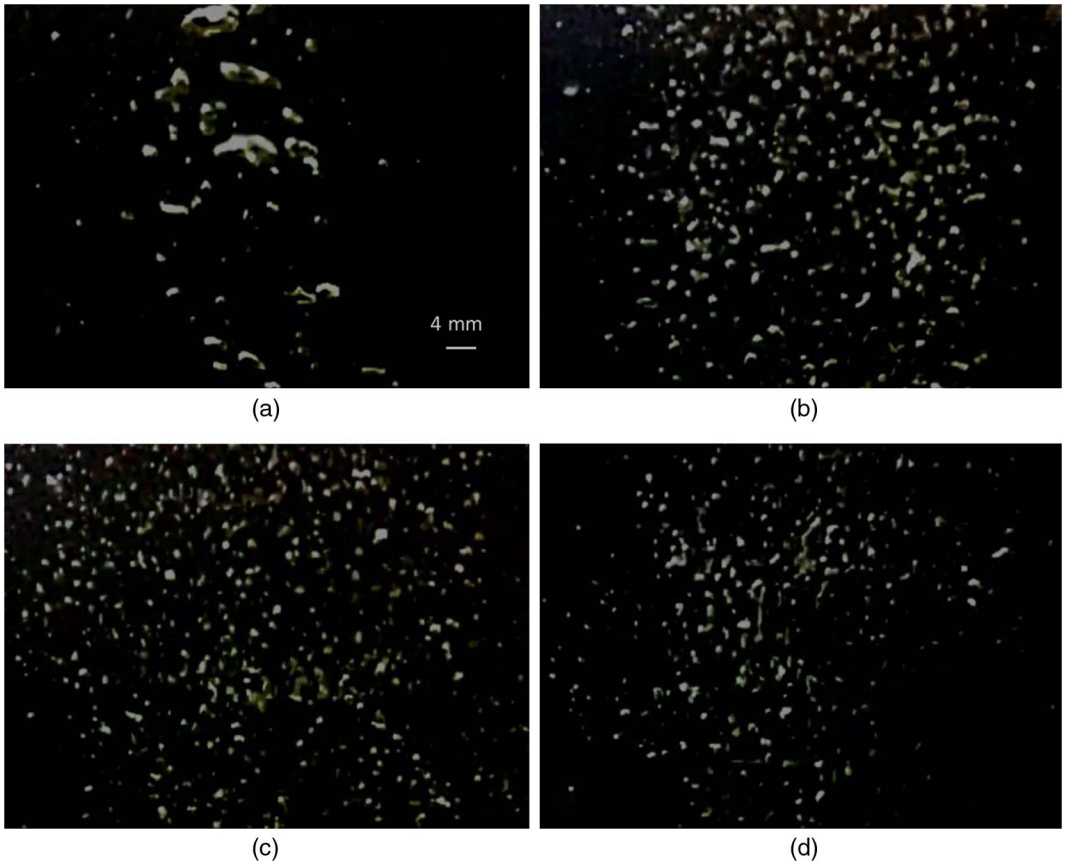

Fig. 4. Typical images of bubbles: (a) Experiment 2—nozzle A ($d_b = 4.3$ mm); (b) Experiment 6—nozzle B ($d_b = 2.5$ mm); (c) Experiment 10—nozzle C ($d_b = 2.2$ mm); and (d) Experiment 12—nozzle D ($d_b = 1.7$ mm). A length scale of 4 mm is also shown in panel (a) for comparison purposes.

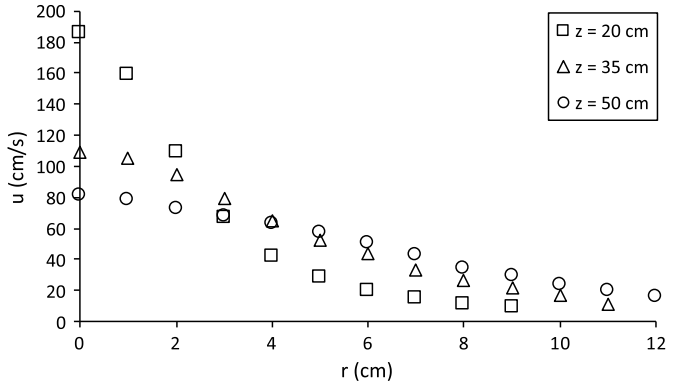

Fig. 5. Radial distribution of axial water velocity measured at different heights: $z = 20$, 35, and 50 cm (Experiment 8).

Baylar and Ozkan (2006) also found similar reductions in $Q_{g,o}/Q_{l,o}$ when longer pipes (resulting in higher friction head losses) were used downstream for the Venturi tubes.

Bubble size distribution computed by using ImageJ followed lognormal curves with mean Sauter diameters d_b ranging from about 1.7–4.8 mm and decreasing from nozzles A to D, as illustrated in Fig. 4. The Reynolds numbers, R_o, were calculated at each nozzle (or at each orifice, for the cases of multiple-orifice nozzles) and varied from about 9,000 to 65,000 (Table 1). Note that $R_o = 4Q_{l,o}/(\pi d_l)$, in which l is the kinematic viscosity of water. The aforementioned bubble diameters are consistent with the condition of Lima Neto et al. (2008b, c), in which $R_o > 8{,}000$ produced bubbles of about 1–4 mm in diameter. Moreover, the bubble diameters were relatively close (−14 to +42%) to those obtained from the correlation of Lima Neto (2015), which is given by $d_b = (0.1 + 0.3 \times 10^4 \varepsilon_o/R_o)L$, where L is a length scale defined as $L = ({Q_{g,o}}^2/g)^{1/5}$. Observe that for the previously mentioned range of bubble diameters ($d_b = 1.7$–4.8 mm), the bubble slip velocity (u_s) can be assumed constant and equal to 0.23 m/s (Wüest et al. 1992; Lima Neto et al. 2016).

Typical radial distributions of axial water velocity (u) measured at different heights (z) are shown in Fig. 5. Self-similar curves resembling Gaussian profiles were observed for all these experiments, as reported in previous single- and two-phase jet/plume studies (Rajaratnam 1976; Milgram 1983; Sun and Faeth 1986; Kumar et al. 1989; Iguchi et al. 1997; Lima Neto 2015). Table 2 shows the values of u_c and b obtained by least squares fitting of Gaussian distributions to the velocity profiles measured at different heights, resulting in average deviations of up to 14%. Fig. 6 shows examples of this curve fitting.

If one now calculates the jet-to-plume length scale $L_m = M_0^{3/4}/B_0^{1/2}$ for each experimental condition, in which $M_o = Q_{l,o}u_o$ and $B_o = Q_{g,o}g(\rho_l - \rho_g)/\rho_l$ are the kinematic fluxes of momentum and buoyancy at the source, and ρ_l and ρ_g are the liquid and gas densities, respectively, values of z/L_m of 6–32 are obtained for the tests with the large nozzle (A), while values of z/L_m of 1–6 are obtained for the tests with the smaller nozzles (B–D). Thus, according to the jet-to-plume transition of $z/L_m \sim 5$–10 defined

Table 2. Centerline velocity (u_c) and jet/plume radius (b, for $u = 0.37u_c$) obtained by fitting Gaussian distributions to the measured velocity profiles

Experiment	z (cm)	u_c (cm/s)	b (cm)
1	50	25	5.8
	35	27	4.7
	20	29	3.5
2	50	31	7.0
	35	33	5.5
	20	36	4.8
3	50	37	8.0
	35	38	6.4
	20	41	4.6
4	50	44	8.0
	35	44	6.3
	20	46	5.0
5	50	46	8.4
	35	48	6.7
	20	49	5.8
6	50	54	7.0
	35	75	6.1
	20	117	3.0
7	50	69	8.2
	35	98	5.9
	20	148	2.9
8	50	82	8.5
	35	110	6.1
	20	186	3.0
9	50	38	6.3
	35	47	4.8
	20	79	3.2
10	50	65	6.8
	35	82	5.8
	20	140	2.8
11	50	81	8.0
	35	105	5.7
	20	175	2.9
12	50	59	7.5
	35	83	5.0
	20	128	3.5
13	50	70	8.7
	35	96	5.6
	20	162	3.7
14	50	95	8.1
	35	120	6.3
	20	208	3.3

by Lima Neto (2012b), all the tests with the large nozzle A can be considered as bubble plumes (or buoyancy-dominated bubbly jets), while the other tests can be considered as bubbly jets (or momentum-dominated bubbly jets). Note that an equivalent diameter based on the total area of the nozzles (including single- and multiple-orifices) was used to estimate the water velocity at the source (u_o), which is needed to calculate M_o. Fig. 7 confirms that experiments with similar ranges of z/L_m present similar dimensionless velocity distributions, with a clear distinction between a jet-like ($z/L_m < 5$) and a plume-like ($z/L_m > 10$) regime. Fig. 7(b) also shows that the number of orifices did not affect significantly the velocity magnitude and distribution in bubbly jets. This may be attributed to the fact that the orifices were close enough to each other (jet initial spacing < 3 cm) to merge the jets below a relatively short distance from the source ($z < 20$ cm), so that the velocity magnitudes and distributions (and L_m) depend only on the total orifice area and not the number of ports. However, the bubbly jets should behave as a group of individual jets for z lower than about 3–4 jet initial spacing, i.e., $z < 9$–12 cm (Lai and Lee 2012).

Fig. 8 shows the least squares fitting of the integral model to the experimental data for different nozzle designs and at a particular height. As already mentioned, constant values for the bubble slip velocity ($u_s = 0.23$ m/s), momentum amplification factor ($\gamma = 1.0$), and spreading ratio of the bubble core ($\lambda = 0.6$) were assumed (Lima Neto 2015). The integral model also fitted well with the other experiment runs in this study, resulting in average deviations between model predictions and experimental data of up to 19%. Similar deviations (<20%) were also obtained by comparing the integral model results to the fitted Gaussian distributions summarized in Table 2. Note that model simulations were insensitive to λ. Overall, the adjusted values of the entrainment coefficient (α) ranged from about 0.04 to 0.10, which are within the values reported by Milgram (1983), Seol et al. (2007), and Lima Neto (2012a, b, 2015). Again, it is seen as a very distinct behavior of the tests with the large nozzle A ($u/u_o \sim 80$), while the tests with the smaller nozzles B–D all produced very similar results ($u/u_o \sim 14$). This reinforces the idea that, for fixed flow rates of liquid and gas, the total area of the orifices independent of the number of ports can change the initial momentum of the bubbly jet and the jet-to-plume length scale of the flow. Observe that the orifice area is a design parameter, while the jet momentum flux is an independent variable that can be controlled.

In order to separate plume (nozzle A) and jet (nozzles B–D) measurements, the fitted entrainment coefficients α are plotted in Fig. 9(a) as a function of the local densimetric Froude number, which is defined as $\mathsf{F} = u_c/(g_c' b)^{0.5}$, where g_c' is the reduced gravity at the jet or plume centerline. The general correlation given by Jirka (2004) for the entrainment coefficient of single-phase jets and plumes ($\alpha = 0.055 + 0.6/\mathsf{F}^2$) is also plotted for comparison. Notably, there is a different behavior between the jet and plume data. The correlation of Jirka (2004) overestimates the values of α in the plume regime, probably because the tests conducted with the large nozzle (A) presented larger bubbles that predominantly occupied the central portion of the flow (Fig. 4), potentially reducing the entrainment from the edges of the plume. Note that similar values within the range of $\alpha = 0.03$–0.12 were also reported by Milgram (1983) and Seol et al. (2007) for bubble plumes. On the other hand, the correlation of Jirka (2004) slightly underestimates the values of α in the jet regime (smaller nozzles B–D), which may be attributed to the additional entrainment into the wakes of the bubbles, as suggested by Lima Neto et al. (2008b).

Hence, to generalize the integral model, curve fitting provided the following functional relationship to describe the entrainment coefficient α as a function of a nondimensional velocity, which is given by the ratio of the bubble slip velocity u_s to a characteristic velocity scale $(B/z)^{1/3}$:

$$\alpha = 0.18 \exp\left(-1.7 \frac{u_s}{\left(\frac{B}{z}\right)^{\frac{1}{3}}}\right) + 0.06 \tag{7}$$

in which B = kinematic flux of buoyancy defined as $B = Q_g g(\rho_l - \rho_g)/\rho_l$. Fig. 9(b) shows the fit of Eq. (7) to the experimental data, which resulted in an average deviation in α of 11%. Error bars also indicate deviations of 5 and 7% obtained by comparing repeatability tests for Experiments 6 and 14, respectively. Note that Eq. (7) has the same form of the entrainment coefficient relationship proposed by Seol et al. (2007) for bubble plumes. The only difference is the constant of 0.06, which is higher than that obtained in the previous study (0.04). However, it is important to point out that the correlation of Seol et al. (2007) was fitted to the experimental data of several studies ranging from small- to large-scale bubble plumes, which exhibits a significant scatter. But Eq. (7) presented a better fit to their own lab data, which

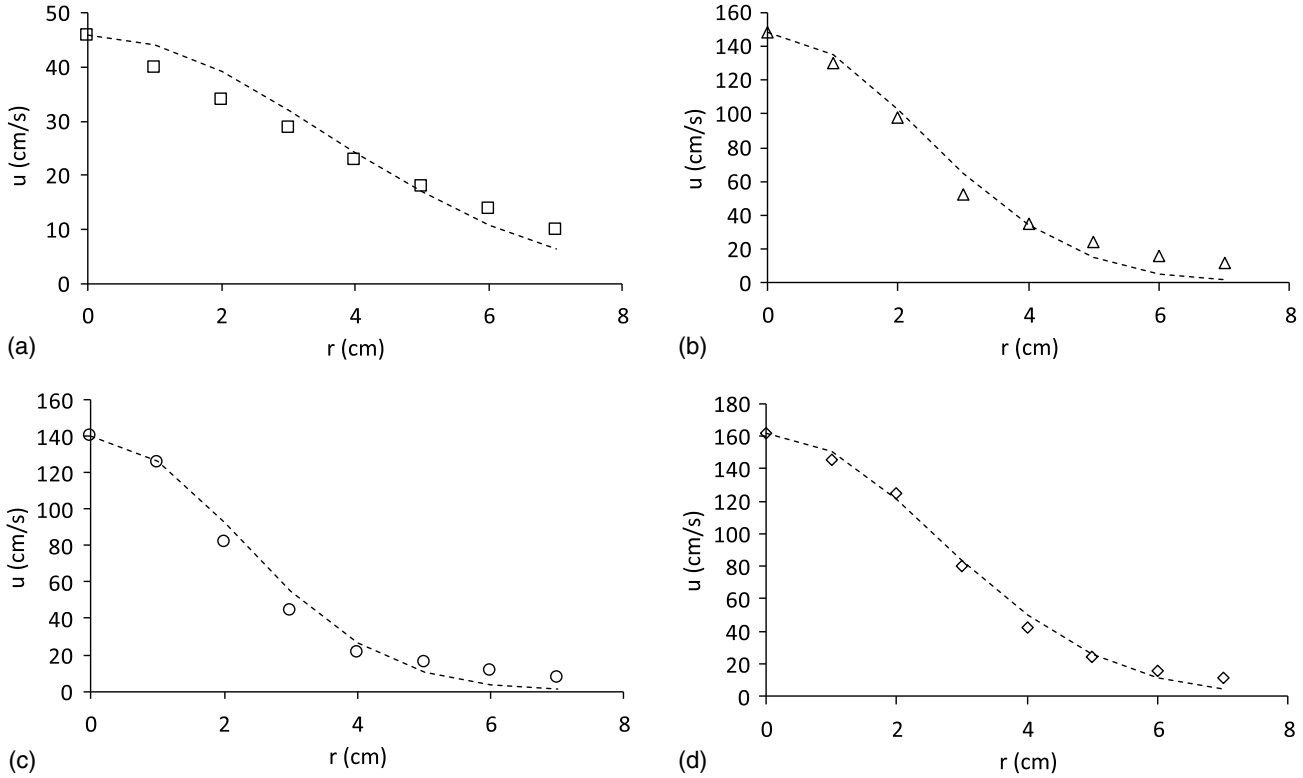

Fig. 6. Fitting of Gaussian distributions to velocity profiles measured at $z = 20$ cm: (a) Experiment 4 (nozzle A); (b) Experiment 7 (nozzle B); (c) Experiment 10 (nozzle C); and (d) Experiment 13 (nozzle D).

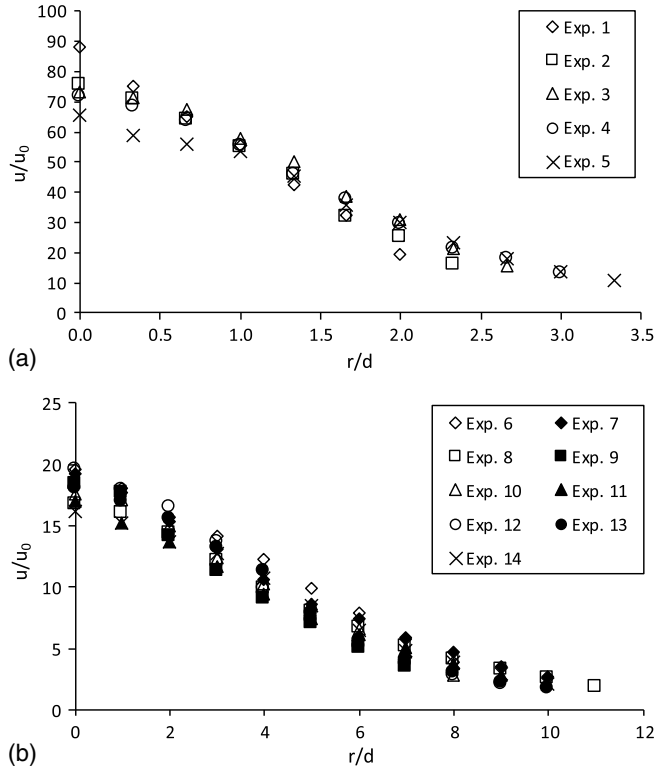

Fig. 7. Normalized radial distributions of axial water velocity measured at $z = 35$ cm: (a) bubble plume experiments with nozzle A ($z/L_m > 10$); and (b) bubbly jet experiments with nozzles B–D ($z/L_m < 5$).

was obtained through detailed particle image velocimetry (PIV) measurements. This suggests that Eq. (7) is a good approximation for both bubble plumes and bubbly jets.

Applications

The integral model and entrainment relationship proposed in this study can be used to estimate the mixing patterns and mass transfer characteristics in tanks and water bodies. For instance, consider a jet aeration system composed of an air-water bubbly jet injected vertically in stagnant water, with the following flow conditions: $Q_{g,o} = 60$ L/min, $Q_{l,o} = 120$ L/min, and $H = 4$ m. Then, if one considers a diffuser (single- or multiple-orifice nozzle) with an equivalent diameter $d = 30$ mm, one can estimate the water flow induced by the bubbly jet along the distance from the source. Fig. 10(a) shows the results of this simulation in comparison with those obtained by using the entrainment coefficient relationships of Seol et al. (2007) and Lima Neto (2012b), and the constant value of $\alpha = 0.077$, as suggested by Lima Neto (2015). It can be seen that this model predicts total entrained fluid volume fluxes that are between 12% and 28% higher than predictions using the other entrainment models. Similar results were also obtained for other flow conditions. The advantage is that this model and that of Seol et al. (2007) can also be used for two-layer stratified water conditions and under the presence of bubble dissolution, where B and u_s can change with z. On the other hand, Fig. 10(b) shows a comparison of the SOTE reached for different diffuser configurations, including single- and multiple-orifice nozzles with the same total area of the orifices. Observe that each diffuser configuration produced a different bubble diameter by using the previously mentioned correlation of Lima Neto (2015): (1) $d_b = 6.8$ mm for a single-orifice nozzle of 30 mm;

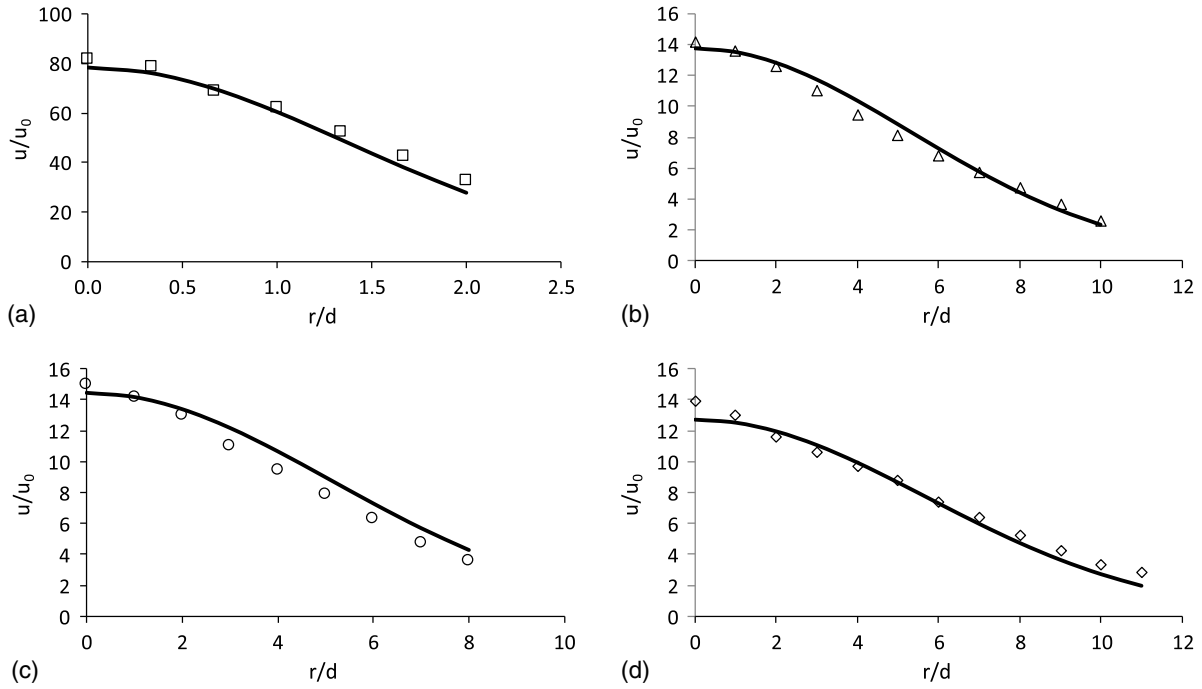

Fig. 8. Fitting of integral model to experimental data at $z = 50$ cm: (a) Experiment 1 (nozzle A); (b) Experiment 6 (nozzle B); (c) Experiment 9 (nozzle C); and (d) Experiment 12 (nozzle D).

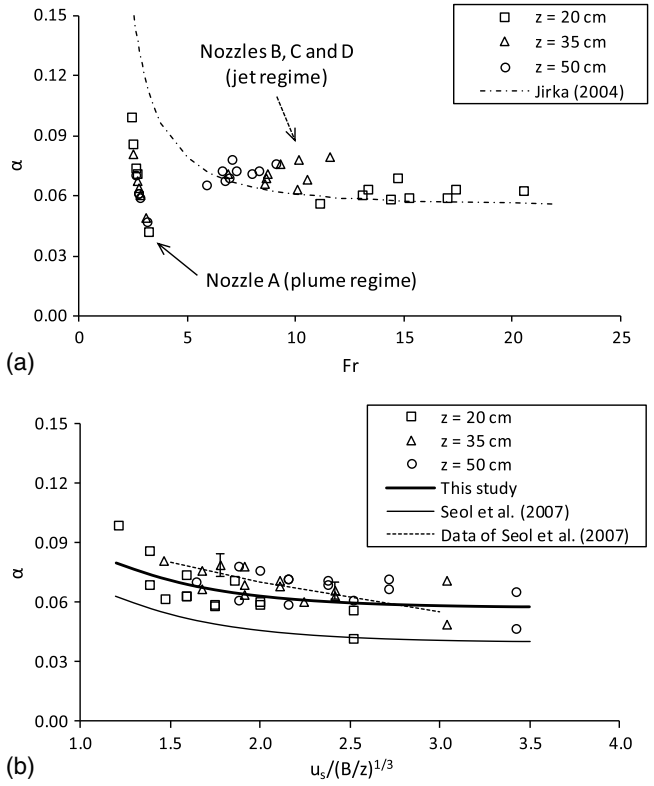

Fig. 9. Relationships for entrainment coefficient considering both jet and plume regimes: (a) as a function of densimetric Froude number; and (b) as a function of nondimensional velocity. In (a), correlation of Jirka (2004) is also shown for comparison. In (b), correlation proposed by Seol et al. (2007) and a curve fitted to their own data are also shown. Error bars indicate typical variations in adjusted entrainment coefficients.

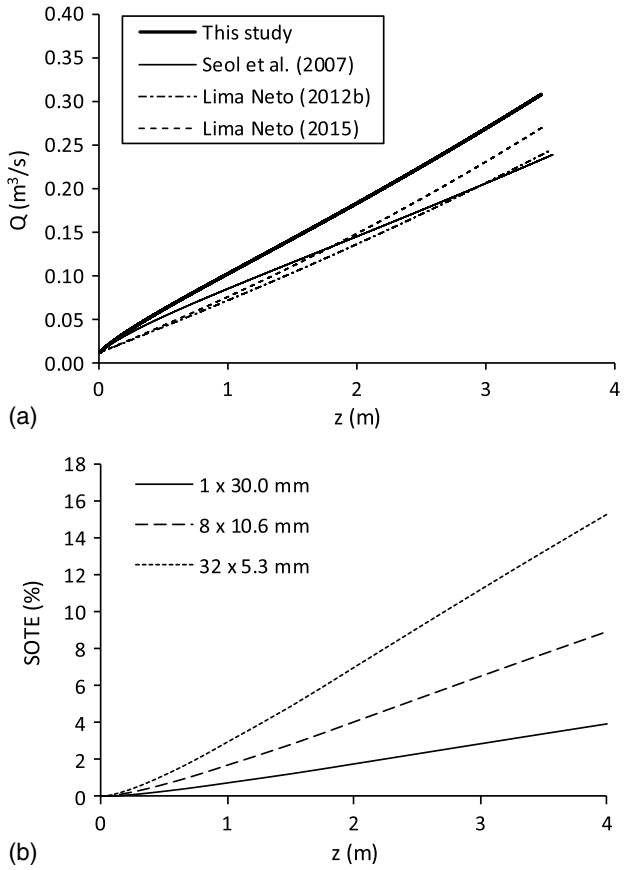

Fig. 10. Model simulations for $d = 30$ mm, $H = 4$ m, $Q_{g,o} = 60$ L/min, and $Q_{l,o} = 120$ L/min: (a) comparison of induced liquid volume flux generated by using different models; and (b) comparison of SOTE for different diffuser configurations, including single- and multiple-orifice nozzles with same total area.

(2) $d_b = 2.9$ mm for a nozzle with eight orifices of 10.6 mm; and (3) $d_b = 1.7$ mm for a nozzle with 32 orifices of 5.3 mm. For such bubble diameters, $u_s = 0.23$ m/s and $K_L = 4 \times 10^{-4}$ m/s (Wüest et al. 1992). The impact of nozzle type on the oxygen transfer efficiency can be clearly seen, with the values of SOTE ranging from about 4–15% for the different diffuser configurations.

Conclusions

This paper studied experimentally the impact of different diffusers, including single- and multiple-orifice and large nozzles, on jet aeration systems. The results indicate that the smaller the equivalent diameter of the nozzles or the larger the number of orifices, the lower the gas-liquid flow ratio incorporated by the Venturi injector and the smaller the bubble diameters generated in the tank. On the other hand, the total area of the orifices sets the characteristic momentum-to-buoyancy length scale L_m, independent of the number of ports, and the nondimensional height z/L_m determines the flow behavior as either a jet ($z/L_m < 5$) or a plume ($z/L_m > 10$) for a given flow condition. Hence, an equivalent diameter based on the total area of the orifices was used to estimate the water velocities at the nozzle exit and fit an integral model to the experimental data, which confirmed that merged multiple bubbly jets can be analyzed using an equivalent single jet integral model. This resulted in entrainment coefficients α ranging from 0.04 to 0.10, which could be described as a function of dimensionless parameters based on the kinematic buoyancy flux, bubble slip velocity. and distance from the source. Finally, this model was compared to previous bubble plume and bubbly jet models, resulting in deviations of up to about 30% of the total liquid volume flux predicted by the other models. On the other hand, the oxygen transfer efficiency increased by up to about 300% when a single-orifice nozzle was replaced by multiple-orifice nozzles with same total area. This indicates that multiple-orifice diffusers can be used to control the bubble size and improve the oxygen transfer efficiency compared to that of an equivalent single-orifice diffuser, with the same initial momentum and buoyancy fluxes.

Acknowledgments

The authors are grateful to the Brazilian National Council for Scientific and Technological Development—CNPq for the Ph.D. scholarship granted to D. D. Lima and for the financial support of this study (Project No. 445211/2014-8). The authors also thank Mr. Ernane Gadelha for building the experimental apparatus.

References

Baylar, A., and F. Ozkan. 2006. "Applications of venturi principle to water aeration systems." *Environ. Fluid Mech.* 6 (4): 341–357. https://doi.org/10.1007/s10652-005-5664-9.

Baylar, A., F. Ozkan, and M. Unsal. 2007. "On the use of venturi tubes in aeration." *Clean* 35 (2): 183–185. https://doi.org/10.1002/clen.200600025.

Freire, A. P. S., D. D. E. Miranda, L. M. S. Luz, and G. F. M. França. 2002. "Bubble plumes and the Coanda effect." *Int. J. Multiphase Flow* 28 (8): 1293–1310. https://doi.org/10.1016/S0301-9322(02)00031-9.

Iguchi, M., K. Okita, T. Nakatani, and N. Kasai. 1997. "Structure of turbulent round bubbling jet generated by premixed gas and liquid injection." *Int. J. Multiphase Flow* 23 (2): 249–262. https://doi.org/10.1016/S0301-9322(96)00060-2.

Jirka, G. H. 2004. "Integral model for turbulent buoyant jets in unbounded stratified flows. Part I: Single round jet." *Environ. Fluid Mech.* 4 (1): 1–56. https://doi.org/10.1023/A:1025583110842.

Kaye, N. B., and P. F. Linden. 2004. "Coalescing axisymmetric turbulent plumes." *J. Fluid Mech.* 502: 41–63. https://doi.org/10.1017/S0022112003007250.

Kumar, S., D. N. Nikitopoulos, and E. E. Michaelides. 1989. "Effect of bubbles on the turbulence near the exit of a liquid jet." *Exp. Fluids* 7: 487–494. https://doi.org/10.1007/BF00187067.

Lai, A, C., and J. H. Lee. 2012. "Dynamic interaction of multiple buoyant jets." *J. Fluid Mech.* 708: 539–575. https://doi.org/10.1017/jfm.2012.332.

Lima Neto, I. E. 2012a. "Bubble plume modelling with new functional relationships." *J. Hydraul. Res.* 50 (1): 134–137. https://doi.org/10.1080/00221686.2011.651278.

Lima Neto, I. E. 2012b. "Modeling the liquid volume flux in bubbly jets using a simple integral approach." *J. Hydraul. Eng.* 210–215. https://doi.org/10.1061/(ASCE)HY.1943-7900.0000499.

Lima Neto, I. E. 2015. "Self-similarity of vertical bubbly jets." *Braz. J. Chem. Eng.* 32 (2): 475–487. https://doi.org/10.1590/0104-6632.20150322s00003371.

Lima Neto, I. E., S. S. S. Cardoso, and A. W. Woods. 2016. "On mixing a density interface by a bubble plume." *J. Fluid Mech.* 802: R3 https://doi.org/10.1017/jfm.2016.454.

Lima Neto, I. E., and P. A. B. Parente. 2016. "Influence of mass transfer on bubble plume hydrodynamics." *Ann. Braz. Acad. Sci.* 88 (1): 411–422. http://doi.org/10.1590/0001-3765201520140453.

Lima Neto, I. E., and R. M. Porto. 2004. "Performance of low-cost ejectors." *J. Irrig. Drain. Eng.* 130 (2): 122–128. https://doi.org/10.1061/(ASCE)0733-9437(2004)130:2(122).

Lima Neto, I. E., D. Z. Zhu, and N. Rajaratnam. 2008a. "Air injection in water with different nozzles." *J. Environ. Eng.* 134 (4): 283–294. https://doi.org/10.1061/(ASCE)0733-9372(2008)134:4(283).

Lima Neto, I. E., D. Z. Zhu, and N. Rajaratnam. 2008b. "Bubbly jets in stagnant water." *Int. J. Multiphase Flow* 34 (12): 1130–1141. https://doi.org/10.1016/j.ijmultiphaseflow.2008.06.005.

Lima Neto, I. E., D. Z. Zhu, and N. Rajaratnam. 2008c. "Horizontal injection of gas-liquid mixtures in a water tank." *J. Hydraul. Eng.* 134 (12): 1722–1731. https://doi.org/10.1061/(ASCE)0733-9429(2008)134:12(1722).

Lima Neto, I. E., D. Z. Zhu, N. Rajaratnam, T. Yu, M. Spafford, and P. McEachern. 2007. "Dissolved oxygen downstream of an effluent outfall in an ice-covered river: Natural and artificial aeration." *J. Environ. Eng.* 133 (11): 1051–1060. https://doi.org/10.1061/(ASCE)0733-9372(2007)133:11(1051).

Milgram, J. H. 1983. "The mean flow in round bubble plumes." *J. Fluid Mech.* 133 (Aug): 345–376. https://doi.org/10.1017/S0022112083001950.

Mueller, J. A., W. C. Boyle, and H. J. Pöpel. 2002. *Aeration: Principles and practice*. New York, NY: CRC Press.

Pacheco, C. H. A., and I. E. Lima Neto. 2017. "Effect of artificial circulation on the removal kinetics of cyanobacteria in a hypereutrophic shallow lake." *J. Environ. Eng.* 143 (12): 06017010. https://doi.org/10.1061/(ASCE)EE.1943-7870.0001289.

Rajaratnam, N. 1976. *Turbulent jets*. Amsterdam, Netherlands: Elsevier Scientific.

Schierholz, E. L., J. S. Gulliver, S. C. Wilhelms, and H. E. Henneman. 2006. "Gas transfer from air diffusers." *Water Res.* 40 (5): 1018–1026. https://doi.org/10.1016/j.watres.2005.12.033.

Schneider, C. A., W. S. Rasband, and K. W. Eliceiri. 2012. "NIH Image to ImageJ: 25 years of image analysis." *Nat. Methods* 9 (7): 671–675. https://doi.org/10.1038/nmeth.2089.

Seol, D.-G., T. Bhaumik, C. Bergmann, and S. A. Socolofsky. 2007. "Particle image velocimetry measurements of the mean flow characteristics in a bubble plume." *J. Eng. Mech.* 133 (6): 665–676. https://doi.org/10.1061/(ASCE)0733-9399(2007)133:6(665).

Sun, T. Y., and G. M. Faeth. 1986. "Structure of turbulent bubbly jets—I: Methods and centerline properties." *Int. J. Multiphase Flow* 12 (1): 99–114. https://doi.org/10.1016/0301-9322(86)90006-6.

Wüest, A., N. H. Brooks, and D. M. Imboden. 1992. Bubble plume modeling for lake restoration *Water Resour. Res.* 28 (12): 3235–3250. https://doi.org/10.1029/92WR01681.

Zhang, W., and D. Z. Zhu. 2014. "Trajectories of air-water bubbly jets in crossflows." *J. Hydraul. Eng.* 140 (7): 06014011. https://doi.org/10.1061/(ASCE)HY.1943-7900.0000886.